The RNA-binding protein Rrm4 is essential for polarity in *Ustilago maydis* and shuttles along microtubules

Philip Becht*, Julian König* and Michael Feldbrügge‡

Max Planck Institute for Terrestrial Microbiology, Department for Organismic Interactions, Karl-von-Frisch-Str., 35043 Marburg, Germany

*These authors contributed equally to this work

‡Author for correspondence (e-mail: feldbrue@mpi-marburg.mpg.de)

Accepted 2 October 2006
Journal of Cell Science 119, 4964-4973 Published by The Company of Biologists 2006
doi:10.1242/jcs.03287

Summary

Formation of polar-growing hyphae is essential for infection by the plant pathogen *Ustilago maydis*. Here we observe that loss of RNA-recognition motif protein Rrm4 caused formation of abnormal hyphae. The insertion of septa at the distal pole was abolished and a significantly increased number of hyphae grew bipolarly. UV-crosslinking experiments revealed that Rrm4 bound RNA via its N-terminal RRMs and that its RNA-binding activity was substantially increased during filamentation. Rrm4 assembled into particles that shuttled bidirectionally along microtubules to both poles. Recruitment of Rrm4 into particles increased during filamentation, and mutations in the peptide-binding pocket of its PABC domain caused abnormal particle formation as well as polarity defects. Shuttling was mediated by active transport because loss of conventional kinesin, which interferes with the balance of microtubule-dependent motors, caused accumulation of particles at the poles resulting in disturbed polarity. Thus, constant transport of the RNA-binding protein towards the poles is needed to orchestrate hyphal growth. Since a mutation of the N-terminal RRM that leads to reduced RNA binding in vivo also affected polarity, Rrm4 might regulate polarity of the infectious hyphae by transporting RNA from the nucleus to cell poles.

Supplementary material available online at
http://jcs.biologists.org/cgi/content/full/119/23/4964/DC1

Key words: RNA-recognition motif, Microtubule-dependent transport, Ribonucleoprotein particles, Plant pathogen

Introduction

Ustilago maydis causes smut disease on corn. Aside from the human pathogen *Cryptococcus neoformans* it represents the model system of choice for pathogenic basidiomycetes (Feldbrügge et al., 2004; Hull and Heitman, 2002). Prerequisite for plant infection is mating of two haploid sporidia resulting in the formation of a filamentously growing dikaryon – the infective form. This developmental switch is elicited by a pair of homeodomain transcription factors, bE and bW, which are only functional as heterodimers after cell fusion of compatible mating partners (Kämper et al., 1995). Infectious hyphae grow polarly by expanding at the apical tip and inserting regularly spaced septa at the distal pole resulting in the formation of characteristic empty sections (Steinberg et al., 1998). This growth mode enables the fungus to progress along the plant surface most likely to find an appropriate point of entry. Cell biological analyses revealed that microtubule-dependent transport processes are essential to support polar growth. Treatment of filamentously growing cells with the microtubule inhibitor benomyl caused growth inhibition (Fuchs et al., 2005) and deletion of *kin1* encoding the conventional kinesin, a microtubule-dependent motor, resulted in increasing numbers of bipolarly growing cells and an absence of empty sections (initially published as *kin2*) (Lehmler et al., 1997; Schuchardt et al., 2005; Steinberg et al., 1998). At present, no molecular cargo for microtubule-dependent transport has been identified. However, the involvement of early endosomes shuttling along microtubules during polar growth suggests the participation of vesicular transport. Thus, endocytotic membrane recycling might be needed for local exocytosis (Steinberg and Fuchs, 2004).

Recently, we have shown that RNA-binding proteins are implicated in pathogenic development. In particular, the deletion of *rrm4* resulted in shorter infectious hyphae and induced fewer and smaller tumours (Becht et al., 2005). The encoded RNA-binding protein displays a novel domain architecture, consisting of three N-terminal RNA-recognition motifs (RMMs) with typical spacing known from ELAV-like proteins and an additional C-terminal PABC domain. The RRM is the most widespread RNA-binding domain and consists of two conserved RNA contact regions, designated RNP1 and RNP2 (Maris et al., 2005). The PABC domain is a characteristic feature of eukaryotic poly(A)-binding proteins but is also found in HECT E3 ubiquitin ligases (Kozlov et al., 2004; Kozlov et al., 2001). The human PABC domain is not essential for binding of the poly(A) tail but forms a hydrophobic peptide binding pocket for a well-defined PABP-associated motif PAM2 (Albrecht and Lengauer, 2004; Kozlov et al., 2004).

The majority of known RNA-binding proteins regulate posttranscriptional expression. Every step during the life cycle of a eukaryotic mRNA, such as processing, nuclear export, translation, localisation and degradation, is dependent on the interaction with distinct RNA-binding proteins (Moore, 2005). Evidence is increasing that they often function as part of large ribonucleoprotein complexes, designated RNP granules or particles (Anderson and Kedersha, 2006; Dreyfuss et al., 2002).

In the current study we investigate the function of the RNA-binding protein Rrm4 during pathogenic development. We demonstrate that its RNA-binding activity as well as its assembly into moving particles are important to determine polarity. Thus, we assume that Rrm4 mediates long-distance RNA transport.

Results

rrm4Δ filaments are disturbed in polar growth

RNA-binding proteins have been implicated in pathogenic development of *U. maydis*. Loss of Rrm4 resulted in reduced disease symptoms and shorter dikaryotic filaments on plates (Becht et al., 2005). To investigate the latter mutant phenotype in more detail we used the laboratory strain AB33 that is well suited to study filamentation. This haploid strain expresses an active bW2/bE1 heterodimeric transcription factor under control of the nitrate-inducible *nar1* promoter (Brachmann et al., 2001). Thus, *b*-dependent filament formation can be elicited by changing the nitrogen source of the medium. The resulting monokaryotic filament mimics its dikaryotic counterpart in all aspects of filamentous growth (Steinberg et al., 1998): apical tip expansion, nuclear migration, as well as formation of septa and empty sections at the distal pole (Fig. 1B) (Brachmann et al., 2001; Schuchardt et al., 2005).

Initially, we deleted the complete open reading frame (ORF) of *rrm4* in AB33. As a control we replaced the deletion allele with *rrm4G* encoding a C-terminal fusion protein with the enhanced version of the green fluorescent protein (eGFP) under control of the homologous *rrm4* promoter. When grown on plates under inducing conditions AB33 and AB33rrm4G grew filamentously. In comparison, AB33rrm4Δ formed colonies with shorter filaments (Fig. 1A). This was consistent with earlier results observing shorter dikaryotic filaments in crossings of mating-compatible *rrm4Δ* strains (Becht et al., 2005).

On cellular level, AB33rrm4Δ cells were disturbed in *b*-dependent polar growth (Fig. 1B). In contrast to AB33 or AB33rrm4G, filaments of AB33rrm4Δ were retarded in growth (data not shown), failed to insert empty sections (Fig. 1C) and the number of bipolarly growing filaments increased significantly (~threefold; Fig. 1D). Although growth was retarded in *rrm4* deletion strains, after 6 hours of induction, the maximal length of the living tip cell did not differ in AB33, AB33rrm4Δ and AB33rrm4G (Fig. 1E). In summary, the deletion of *rrm4* in AB33 abolished formation of empty sections at the distal pole and increased the number of bipolar cells indicating disturbed polarity.

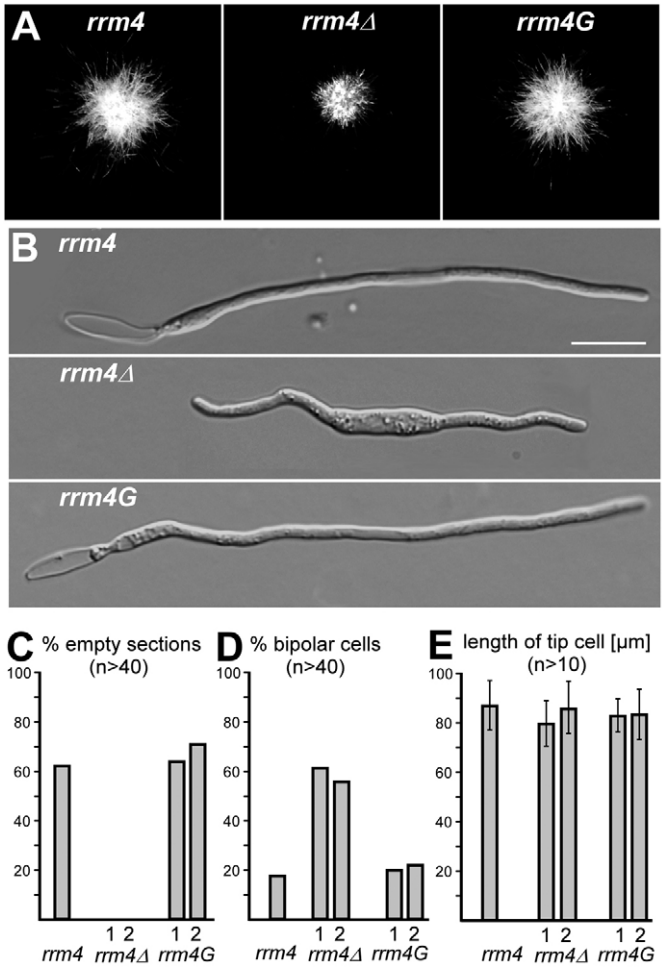

Fig. 1. Loss of Rrm4 causes polarity defects in filaments. (A) Colonies of AB33 and derivatives 24 hours after filament induction on charcoal-containing minimal medium plates (respective *rrm4* alleles labelled at the top). (B) Filament formation was elicited in strains AB33, AB33rrm4Δ and AB33rrm4G for 4 hours in nitrate-containing minimal medium resulting in the *nar1*-promoter-mediated expression of an active bW2/bE1 heterodimer. Bar, 10 µm. (C) Graph indicating the percentage of filaments with empty sections 6 hours after filament induction. More than 40 filaments were analysed each (relevant *rrm4* alleles and number of transformant below). (D) Graph (labelling as in C) indicating the percentage of cells that grew bipolarly 4 hours after filament induction. (E) Graph (labelling as in C) showing the length of the living tip cells of AB33 and derivatives measured 6 hours after filament induction (error bars indicate s.d., more than ten filaments were analysed for each strain).

RNA binding of Rrm4 increases significantly during filamentous growth

Rrm4 had been predicted to be an RNA-binding protein because of sequence similarities to known RRM-containing proteins (Fig. 2A,B) (Becht et al., 2005). To verify this we used a modified version of the in vivo UV crosslinking and immunoprecipitation procedure (CLIP) (Ule et al., 2003) described in the Materials and Methods. We generated strain AB33rrm4GT expressing a Rrm4G fusion protein with a C-terminal tandem affinity purification tag (Tap tag) (Rigaut et al., 1999) and confirmed that Rrm4GT was fully functional (data not shown). Filaments grown for 6 hours under inducing conditions were irradiated with UV doses known to result in covalent bond formation between RNA and proteins (Ule et al., 2003). Subsequently, Rrm4GT was affinity purified. Nucleic acids covalently bound to Rrm4GT were radioactively labelled and detected after membrane blotting (Fig. 2C). The radioactively labelled material was crosslinked RNA, because binding was dependent on UV irradiation and was affected by RNase treatment. RNase T1 cleavage before radioactive labelling resulted in less smear with lower electrophoretic mobility causing sharper signals, because the RNA component of the complex was shortened (Fig. 2C, lanes 2-4). RNase A cleavage after radioactive labelling removed labelled RNA

almost to completion (Fig. 2C, lanes 6-8). This proves that Rrm4GT binds RNA in vivo.

To test whether the activity of Rrm4 is regulated during filamentous growth, we determined Rrm4G as well as Rrm4GT expression in whole cell extracts. Expression of both Rrm4 versions was not altered during the morphological switch indicating that activity of this RNA-binding protein is not regulated on the level of protein expression (Fig. 2D). However, UV-crosslinking experiments comparing polar-growing filaments with budding cells revealed a sevenfold increase of Rrm4GT-bound RNA in filaments (Fig. 2E, lane 1,2). Thus either the capacity to bind RNA might be modified at the posttranslational level or the amount of target RNA might increase during filamentation.

To investigate the contribution of individual Rrm4 domains to RNA binding we analysed mutated versions of Rrm4GT. In its N terminus, Rrm4 contains two tandem RRMs (RRM1 and RRM2) and a third RRM (RRM3) separated by a hinge region (Fig. 2A). Since it is likely that tandem RRMs function in concert for RNA binding (Deo et al., 1999; Handa et al., 1999; Wang and Tanaka Hall, 2001), we analysed only RRM1 and RRM3. Four adjacent amino acids in the conserved RNP1 regions were substituted by alanine (alleles *rrm4GT*^{mR1} and *rrm4GT*^{mR3}, Fig. 2B). Comparable mutations have been reported to destroy RNA binding in Pab1p (Deardorff and Sachs, 1997). In the case of the PABC domain, we introduced point mutations in four conserved amino acids that were known from the human PABC domain to be structurally important (*rrm4GT*^{mP}, Fig. 2B) (Kozlov et al., 2004; Kozlov et al., 2001). The mutant alleles were used to replace *rrm4* in

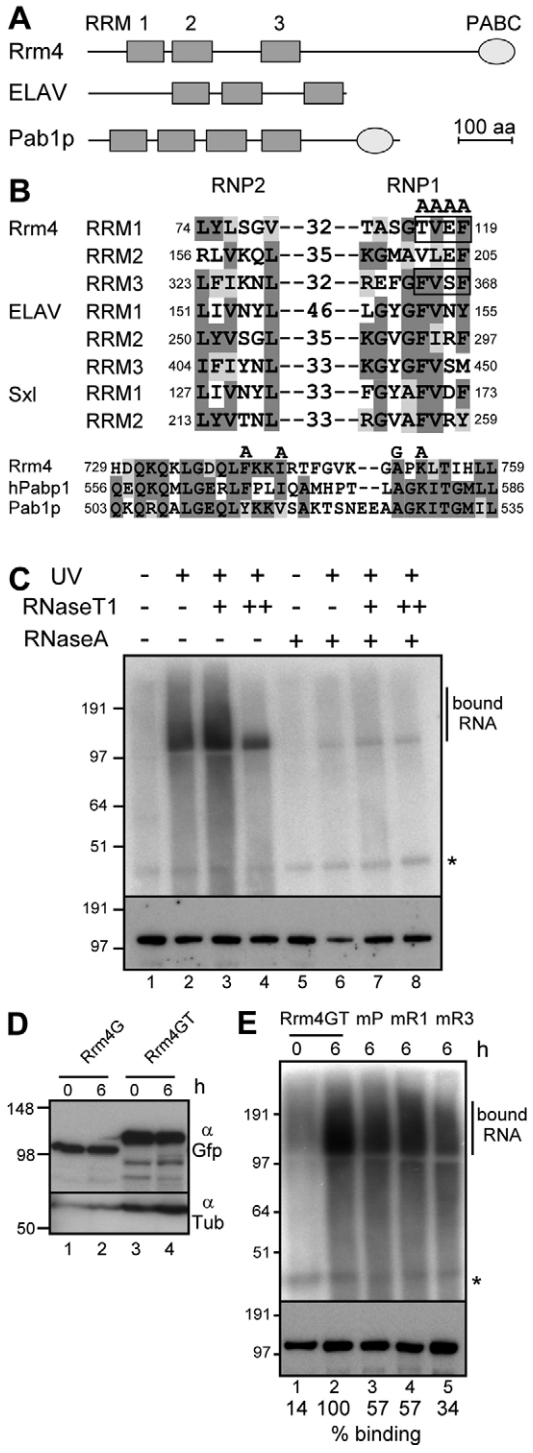

Fig. 2. Rrm4GT binds RNA in vivo probably via N-terminal RRMs. (A) ELAV-like protein Rrm4 contains a unique domain architecture. Domain organisation of RRM-containing proteins is depicted schematically. RRM and PABC domains are indicated as rectangles and ovals, respectively. Accession numbers: ELAV, *D. melanogaster*; P16914; Pab1p, *S. cerevisiae*; P04147; Rrm4, *U. maydis*; UM10836 (http://mips.gsf.de/genre/proj/ustilago/). (B) Sequence comparisons of RRMs and PABC domains are given. The conserved RNP1 and RNP2 regions of RRM proteins Rrm4 from *U. maydis* as well as ELAV and Sex-lethal (Sxl) from *D. melanogaster* are compared (accession numbers UM10836, http://mips.gsf.de/genre/proj/ustilago/, P16914 and Q24668, respectively). Numbers given in small and large fonts indicate amino acid positions and distance between RNP1 and RNP2, respectively. To generate loss-of-function mutants, the boxed sequence in the RNP1 regions of RRM1 and RRM3 were mutated to alanine. Below, the conserved core sequence of the Rrm4 PABC domain is compared with those of poly(A)-binding proteins from human and *S. cerevisiae* (accession numbers UM10836, AAH23520, and AAA34838, respectively). Amino acids above the Rrm4 sequence indicate point mutations in critical amino acids shown to be structural and functionally important in the human PABC domain (Kozlov et al., 2004). Dark and light shading indicate identical and similar amino acids, respectively. (C) Modified CLIP analysis of AB33rrm4GT filaments 6 hours after induction. Covalently bound RNA is detected as radioactively labelled protein-RNA complexes larger in size than Rrm4GT (117 kD after TEV cleavage; size markers are shown on the left; asterisk, unspecific band). Increasing amounts of RNase T1 treatment (lanes 3-4; ++ indicates 100-fold increase) before labelling reduces the size of the bound RNA resulting in a sharper band. RNase A treatment after labelling (lanes 5-8) removes the radioactive signal indicating that the crosslinked material is RNA. Equal loading was verified by western blotting using anti-GFP antibodies on the same membrane (bottom). (D) Western blot experiments using anti-GFP antibodies showing equal protein amounts of Rrm4G and Rrm4GT detected at the onset (0) or after 6 hours of filamentation. Equal loading was verified using anti-α-tubulin antibodies (size markers are shown in kDa on the left). (E) CLIP experiments as in C using AB33rrm4GT (0 and 6 hours after filament induction) and variants expressing mutant alleles *rrm4GT*^{mP} (mP), *rrm4GT*^{mR1} (mR1) and *rrm4GT*^{mR3} (mR3) (6 hours after filament induction). Relative RNA binding (%) was quantified after phosphoimaging.

AB33 resulting in strains AB33rrm4GT^{mR1}, AB33rrm4GT^{mR3} and AB33rrm4GT^{mP}. We verified that none of these mutations affected expression of Rrm4 by western blot experiments (data not shown). UV-crosslinking experiments using these strains revealed that mutations in RRM1, RRM3 and PABC led to a reduction of RNA binding compared with Rrm4GT (two- to threefold; Fig. 2D, lanes 3-5). Hence, intact RNA contact regions of RRM1 and RRM3 as well as an intact peptide-binding pocket of the PABC domain are important for RNA binding in vivo. In summary, Rrm4GT probably forms contacts with RNA in vivo via its N-terminal RRMs and this RNA-binding activity increases significantly during polar growth.

Rrm4 shuttles in particles along defined cytoskeletal tracks

To address the molecular function of Rrm4 we analysed its subcellular localisation in vivo. We used AB33rrm4G, which expresses a functional fusion protein of Rrm4 and eGFP (see above). Rrm4G accumulated in cytoplasmic particles that shuttled along defined cytoskeletal tracks within budding cells (data not shown) as well as in filaments (Fig. 3A; supplementary material Movie 1). In filaments, Rrm4G-containing particles moved bidirectionally with a speed of 1.6±0.7 μm/second (n=40; band width 0.5-3.6 μm/second). The shuttling of particles was observed throughout the entire filament, from the central region around the nucleus to both poles. During a constant time period, comparable numbers of particles passed a zone of reference (6.5 μm in length; 10 μm from the apical pole) in anterograde or retrograde fashion (48% and 46% anterograde as well as 52% and 54% retrograde, in AB33rrm4G#1 and #2, respectively; n>120). No net accumulation of particles in any subcellular region was detectable (Fig. 3A; supplementary material Movie 1).

Comparing budding cells with filaments revealed that the total number of particles within each cell increased tenfold from ~5 to 50 (median values 4 and 5 in budding cells; 55 and 50 in filaments, in AB33rrm4G#1 and #2, respectively; n>200). However, the particle density increased only slightly (1.3-fold in the case of AB33rrm4G#1, i.e. 0.53 and 0.71 particles per μm in budding cells and filaments, respectively; Fig. 3B) indicating that the increase in the number of particles is directly proportional to the cell volume of filaments. Interestingly, we observed that the relative fluorescence intensity of particles is ~twofold higher in filaments compared with budding cells (Fig. 3C) suggesting that during filamentation more Rrm4G is recruited to particles. In essence, Rrm4G accumulates in particles that move bidirectionally along defined cytoskeletal tracks.

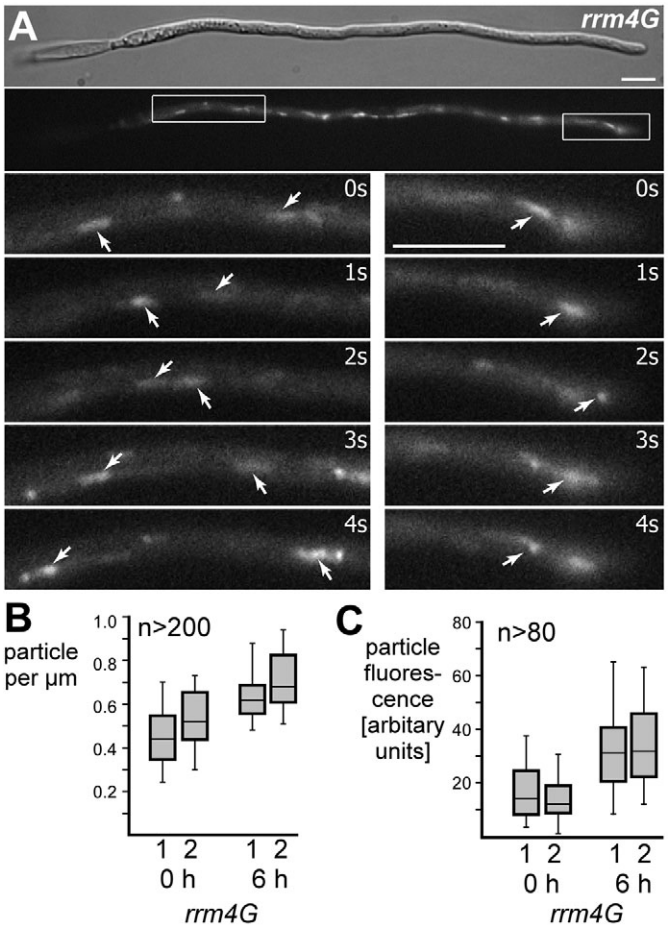

Fig. 3. Rrm4G is assembled into cytoplasmic particles that shuttle along cytoskeletal tracks. (A) AB33rrm4G filaments are shown 4 hours after induction. Epifluorescence images are taken from time-lapse Movie 1 in supplementary material. Rectangles indicate regions that are magnified below. Arrows indicate particles that move along cytoskeletal tracks at the distal pole (left panels) and at the tip (right panels; time in seconds). Bars, 5 μm. (B) Whisker diagram indicating density of Rrm4G-containing particles (particles/μm) in strain AB33rrm4G measured at the onset or after 6 hours of filamentation. The top and bottom of each rectangle represent the 75th and 25th percentiles, respectively. The median is the horizontal line within the box, and the top and bottom borders of the whiskers show the 95th and 5th percentiles, respectively. More than 200 particles were analysed for each strain. The number of the transformant is given below. (C) Whisker diagram (labelling as in B) showing the relative fluorescence intensity of Rrm4G-containing particles in strain AB33rrm4G measured at the onset or after 6 hours of filamentation. More than 80 particles each were analysed (number of transformant is indicated below).

The formation of moving particles is important for function

To test the contribution of different domains of Rrm4 to particle formation and function, we generated strains AB33rrm4G^{mP}, AB33rrm4G^{PΔ}, AB33rrm4G^{mR1} and AB33rrm4G^{mR3} analogous to AB33rrm4G (see above). The mutations were identical to those in Rrm4GT (Fig. 2B) with the exception of *rrm4G^{PΔ}*, which carried a 102-residue deletion removing the whole PABC domain. Microscopic analyses of AB33rrm4G^{PΔ} and AB33rrm4G^{mP} filaments revealed in both cases defects in polar growth comparable to that in the *rrm4Δ* mutant, i.e. increased number of bipolar cells and hardly any filaments with distal septa and empty sections (Fig. 4A,B). In filaments of AB33rrm4G^{PΔ} (data not shown) and AB33rrm4G^{mP} the number of Rrm4G-containing particles was drastically reduced and the few remaining particles were non-motile and larger in size (Fig. 4C). Interestingly, a slight increase in cytoplasmic fluorescence was detectable around the nuclear region.

Analysis of AB33rrm4G^{mR3} revealed that the strain behaved like the wild type in terms of polar growth and shuttling of

Rrm4-containing particles (Fig. 4; supplementary material Movie 2). By contrast, strain AB33rrm4G^{mR1} exhibited aberrant filament formation comparable with the *rrm4Δ* strain, i.e. an increased number of bipolar cells and no filaments with empty sections (Fig. 4A,B). Importantly, in strains AB33rrm4G^{mR1} and AB33rrm4G^{mR3} shuttling and fluorescence intensity of Rrm4-containing particles were comparable to the wild type (Fig. 4D; supplementary material Movie 3) suggesting that mutations in RRM1 cause the formation of non-functional particles. In summary, the C-terminal PABC domain of Rrm4 is needed to form moving particles and the N-terminal RNA-contact region of RRM1 is important for particle function.

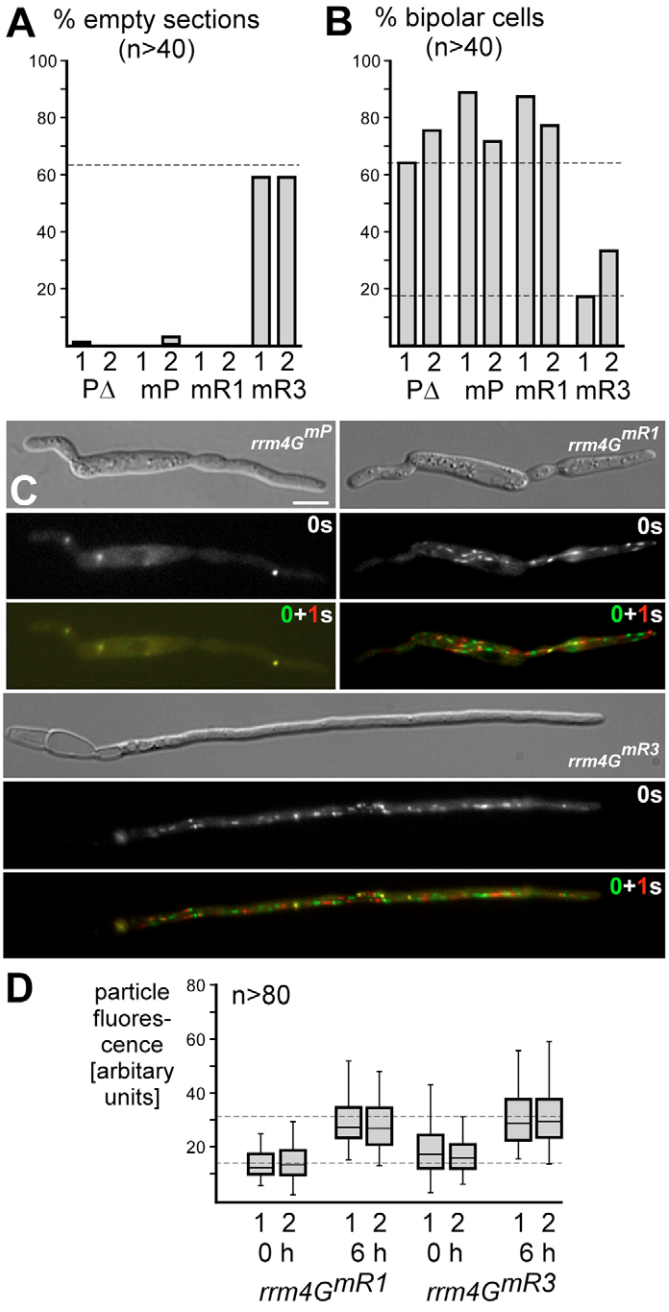

Rrm4-containing particles move along cytoplasmic microtubules

To identify the cytoskeletal tracks along which particles travel we performed inhibitor studies using latrunculin A and benomyl, which interfere with actin and microtubule polymerisation in *U. maydis*, respectively (Fuchs et al., 2005). Treatment of AB33rrm4G filaments with 50 μM latrunculin A for 30 minutes had no influence on Rrm4G particle motility (data not shown). These conditions were previously applied to disturb actin-dependent processes in *U. maydis* (Fuchs et al., 2005). However, treatment of AB33rrm4G filaments with 20 μM benomyl revealed that the motility and number of particles decreased over a period of ~20 minutes (Fig. 5A; supplementary material Movie 4). After this time period, only a few Rrm4G-containing particles remained – these were larger in size and immobile. Washing cells in medium without benomyl resulted in filaments with restored bidirectional movement of Rrm4G-containing particles within 4 minutes (data not shown). Thus, assembly of shuttling Rrm4G-containing particles depends on an intact microtubule cytoskeleton.

This result was verified by in vivo co-localisation studies. We generated strain AB33rrm4R/tub1G expressing a chimera of Rrm4 with the monomeric form of the red fluorescent protein (mRFP, Rrm4R) (Campbell et al., 2002) as a C-terminal fusion at the homologous *rrm4* locus. In addition, the strain expressed an N-terminal fusion of eGFP to α-tubulin Tub1, which was shown to have no influence on cell morphology or filamentation (Tub1G) (Steinberg et al., 2001). In filaments grown for 4 hours under inducing conditions we observed Rrm4R-containing particles that shuttled bidirectionally along dynamic Tub1G-decorated interphase microtubules (Fig. 5B; supplementary material Movie 5).

To exclude the fact that loss of Rrm4 causes aberrant organisation of microtubules, which could be the primary cause for the observed polarity defects, we generated strain AB33rrm4Δ/tub1G carrying a deletion in *rrm4* and expressing a Tub1G chimera. Filaments grown for 6 hours contained the

Fig. 4. The N-terminal RRM1 and the C-terminal PABC domain are important for function. (A) Graph indicating the percentage of filaments with empty sections 4 hours after filament induction (labelling as in Fig. 1C). The mutated alleles of *rrm4* in AB33 derivatives (Fig. 2B) and the number of transformant are given below. More than 40 filaments were analysed for each group. (B) Graph showing the percentage of filaments that grew bipolarly 4 hours after induction (labelling as in A). For comparison the data for *rrm4* and *rrm4Δ* (Fig. 1C,D) are given as dashed lines. (C) Filaments of AB33 derivatives 4 hours after induction. Bar, 5 μm. Frames are taken from supplementary material Movies 2 and 3. To document motility of particles, overlays of two frames that are 1 second apart are shown. The first and second frames are coloured in green and red, respectively, indicating non-motile particles in yellow (top, mutations in PABC) and moving particles in green and red (right and bottom, mutations in RRM). (D) Whisker diagram (labelling as in Fig. 3B) indicating the relative fluorescence intensity of Rrm4G-containing particles in strains AB33rrm4G^{mR1} and AB33rrm4G^{mR3} measured at the onset or after 6 hours of filamentation. For comparison, medians from the data obtained at 0 and 6 hours of filamentation (lower and upper dashed lines, respectively) from AB33rrm4G#1 (data from Fig. 3C) are shown. More than 80 particles were analysed for each group (number of transformant is indicated).

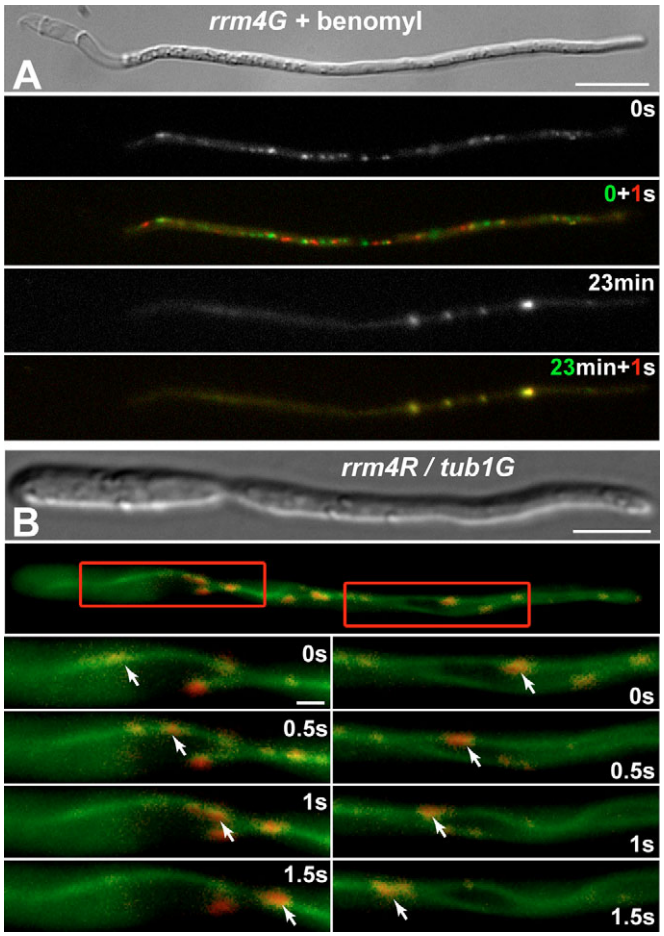

Fig. 5. Rrm4-containing particles shuttle in vivo along microtubules. (A) Filaments of AB33rrm4G were treated with benomyl 4 hours after filament induction and time-lapse movies were taken at the onset (0 seconds, top) and after 23 minutes (bottom) of treatment. Overlays of two frames 1 second apart (coloured in green and red) from supplementary material Movie 4 are shown (moving particles in green and red, top; non-motile particles in yellow, bottom). Bar, 10 μm. (B) In vivo co-localisation of Rrm4R-containing particles (red, arrows) with dynamic Tub1G-decorated microtubules (green) in AB33rrm4R/tub1G filaments 4 hours after induction. Bar, 5 μm. Frames are from supplementary material Movie 5. Rectangles indicate regions that are magnified below. Bar, 1 μm. Time is indicated in seconds.

characteristic number of two to four microtubular bundles, which exhibited typical dynamics comparable with those in filaments of AB33rrm4R/tub1G or wild-type strains (data not shown) (Steinberg et al., 2001). In summary, Rrm4-containing particles shuttle along microtubules to both poles of the filaments.

Conventional kinesin Kin1 is involved in movement of Rrm4 particles

To investigate active transport of Rrm4-containing particles, we treated AB33rrm4G filaments grown for 4 hours under inducing conditions with 100 μM CCCP (carbonyl cyanide m-chlorophenyl-hydrazone), an uncoupler of the oxidative chain that depletes the cytosolic ATP pool. This led to an arrest of particle movement within 5 minutes indicating that ATP-dependent transport is driven by molecular motors (data not shown). To interfere with the function of microtubule-dependent molecular motors we generated strain AB33rrm4G/kin1Δ, carrying a deletion in *kin1*, encoding conventional kinesin. *kin1Δ* strains are known to be disturbed in *b*-dependent filamentation similar to the *rrm4Δ* phenotype (Lehmler et al., 1997; Schuchardt et al., 2005; Steinberg et al., 1998). Consistent with earlier results, this strain did not insert empty sections and a high percentage of filaments grew bipolarly resembling the altered filamentous growth in *rrm4Δ* strains (Fig. 6A). However, analysing the timing of polar growth we observed substantial differences between strains carrying deletions in *kin1* or *rrm4*. In contrast to the latter strain, in *kin1Δ* strains the amount of bipolarly growing cells increased over time. This indicates that *kin1Δ* filaments initially grow unipolar and switch to bipolar growth later (Fig. 6A).

Epifluorescence microscopy revealed that Rrm4G-containing particles accumulated at the cell poles of bipolar growing AB33rrm4G/kin1Δ filaments, whereas they still moved bidirectionally in the central region (Fig. 6B; supplementary material Movie 6). Thus, imbalanced transport of Rrm4-containing particles leads to polarity defects that resemble those observed in *rrm4* deletion strains.

Discussion

A hallmark of hyphal growth in filamentous fungi is the establishment and maintenance of a polar axis. The hyphal tip cell displays a gradient of rapid expansion that peaks at the apical pole. This expanded growth is mediated by the so-called Spitzenkörper, an apical body that is thought to function as a vesicle supply centre needed for active secretion during tip expansion (Harris et al., 2005). The distal pole of the polar growing tip cell is bordered by a septum. In filamentously growing ascomycetes such as *Aspergillus nidulans* or *Neurospora crassa* septa contain pores allowing exchange of cytoplasm and organelles between adjacent compartments (Gladfelter, 2006; Harris et al., 2005). However, other fungi such as the smuts *U. maydis* or *Tilletia laevis* form closed retraction septa confining the cytoplasm to the apical region (Carris et al., 2006; Steinberg et al., 1998). Subcellular organisation of both poles is dependent on molecular transport along microtubules mediated by molecular motors such as dynein and kinesins (Harris et al., 2005). In *U. maydis*, it has been shown that long-distance transport of early endosomes along microtubules is involved in supporting polar growth probably via membrane recycling (Wedlich-Söldner et al., 2000). Here, we observe that the shuttling of a functional RNA-binding protein is essential for septum formation and is important to determine polarity. Thus, our data suggest that in addition to vesicle transport, long-distance transport processes involving RNA-binding proteins are also needed for polar growth of hyphae. This is consistent with earlier observations that clusters of polysomes are closely associated with the Spitzenkörper in tip cells of *Fusarium acuminatum* (Howard, 1981) indicating local mRNA translation.

The RNA-binding activity of Rrm4 is important for determination of polarity

Initially, Rrm4 was predicted to be an RNA-binding protein because of sequence similarities to known RRM-containing

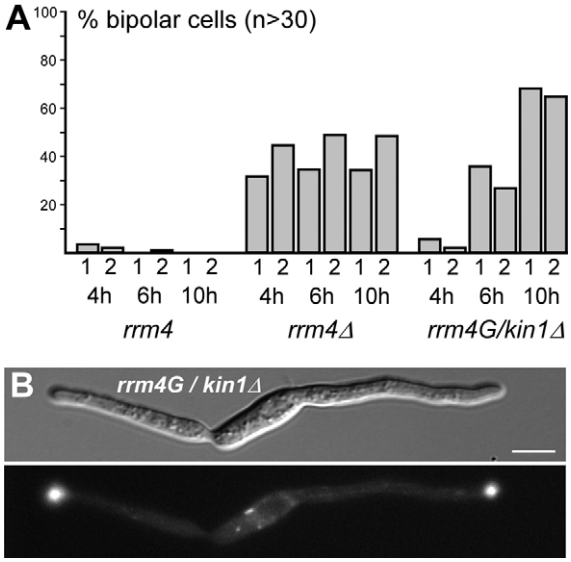

Fig. 6. The loss of Kin1 causes defects in polarity and shuttling of Rrm4G-containing particles. (A) Graph indicating the percentage of filaments that grow bipolarly 4, 6 and 10 hours after induction. More than 30 filaments were analysed for each strain (number of transformant is given below). (B) AB33rrm4G/kin1Δ filaments 6 hours after induction. Epifluorescence image is taken from time-lapse Movie 6 in supplementary material. In bipolar filaments, Rrm4G-containing particles accumulate at the poles. Bar, 5 μm.

proteins (Becht et al., 2005). Here, we demonstrate by UV-crosslinking experiments that Rrm4 binds RNA in vivo. Importantly, RNA binding increases substantially during filamentous growth, suggesting that RNA binding is important at this stage of pathogenic development. Thus, either the RNA-binding activity might be regulated at the posttranslational level or the amount of target RNA increases during filamentation.

Analysing different Rrm4 versions carrying point mutations in conserved regions of RRM1 and RRM3 revealed that the amount of crosslinked RNA was reduced. The strength of our UV-crosslinking approach is that RNA can be detected in close proximity to Rrm4 in vivo. Quantitative comparisons between different mutated Rrm4 versions are difficult, because we cannot differentiate between the alternatives that mutations cause less binding of RNA or that the mutated amino acid side chains mediate crosslinking (Ule et al., 2005). However, in the case of the RRM mutations we can conclude safely that both RNA-contact regions bind RNA in vivo. Our genetic analysis revealed that both RRM1 and RRM3 are dispensable for particle formation, but only RRM1 is functionally important. The observation that RRMs within a single protein can have different functions is already known from other proteins. In the case of the splice factor U2AF^{65}, it has been demonstrated that although its third RRM is not needed for splice activity in vitro, its presence is crucial for viability in *Schizosaccharomyces pombe* (Banerjee et al., 2004). In addition, the third RRM has been implicated in unspecific binding of the poly(A) tail of target mRNAs in ELAV-like proteins mHuC, HuD and HuR (Abe et al., 1996; Ma et al., 1997). In summary, RNA binding is increased during polar growth and RNA contact via RRM1 is functionally important. RRM3 might be dispensable, because it only modulates RNA-binding affinity or binds other RNA sequences whose interaction is not crucial for determining polarity.

Bi-directional movement of Rrm4-containing particles appears to be important for polar growth of infectious hyphae

Subcellular localisation revealed that Rrm4 is a component of particles that move along microtubules. Recruitment of Rrm4 into these particles increases during filamentation. Mutations in the C-terminal PABC domain led to the formation of fewer particles that were larger in size as well as immobile. This resulted in defects in polarity. The PABC domain is a structurally well-defined peptide-binding pocket (Kozlov et al., 2004; Kozlov et al., 2001). At present there are a number of binding partners known to interact with the PABC domain of human PABP such as Paip1, Paip2, eRF3 and Ataxin-2 (Kozlov et al., 2004; Ralser et al., 2005). Therefore, in PABP this domain might function to recruit various translation or mRNA-processing factors to mRNP complexes. In Rrm4, the PABC domain could, for example, be involved in multimerisation or recruitment of microtubule adaptors. Interestingly, this domain also affects RNA binding in vivo, suggesting that the presence of Rrm4 in shuttling particles might be important for RNA interaction.

We observed that Rrm4-containing particles accumulated at the poles in *kin1* deletion strains. A similar finding has been made recently in the same strain for the microtubule-dependent movement of early endosomes. These were also trapped at the filament poles (Lenz et al., 2006). The authors demonstrated that more than 90% of microtubules oriented with their plus end toward the poles in AB33. Thus, it is unlikely that the plus-end-directed motor Kin1 is directly involved in transporting early endosomes to the hyphal tip. Its indirect mode of transport was unravelled by demonstrating that Kin1 is responsible for the transport of the minus-end-directed motor dynein to a loading zone at the plus ends of the microtubules located at hyphal poles (Lenz et al., 2006). This was based on the observations that dynein co-localises only with retrogradely moving endosomes and that this minus-end-directed motor is no longer targeted to the poles in *kin1Δ* strains. Accordingly, Rrm4-containing particles accumulate at the poles in *kin1Δ* strains, because there might not be enough dynein to support retrograde transport.

Deletion of *kin1* or disruption of microtubules with benomyl causes polarity defects in infectious hyphae (Fuchs et al., 2005) indicating that molecular cargos of Kin1 participate in promoting polarity. Similar defects in polarity are observed in *rrm4Δ* strains and in strains expressing non-functional versions of Rrm4. Although Kin1 is most likely involved in transport of multiple molecular cargos, the loss of transport of Rrm4-containing particles could be sufficient to cause polarity defects. The difference in timing of these defects in *rrm4Δ* and *kin1Δ* filaments could be due to the fact that initially Rrm4-containing transport particles still reach the poles in the *kin1Δ* strain. Thus, disturbed polarity is observed later in this strain when recycling of transport particles becomes limiting. These data lend support to the hypothesis that Rrm4-containing particles transport an important molecular cargo to cell poles that functions in determining polarity.

Rrm4 is probably involved in RNA transport

What is the molecular cargo of Rrm4-containing particles? Since RNA binding of Rrm4 is functionally important and because it is generally accepted that RNA-binding proteins shuttling actively along microtubules are involved in RNA transport (St Johnston, 2005), the cargo is probably RNA. This could be tRNA and/or rRNA, whose transport might be needed to enable local translation at the poles to support, for example, protein secretion. Alternatively, Rrm4-containing particles could transport mRNA. Particles might be loaded with mRNA close to the nucleus; these would then transport the cargo to the poles for unloading and shuttle back empty for a new cycle of transport. This scenario might explain how mRNA reaches the ribosomes that are associated with the Spitzenkörper in tip cells of *F. acuminatum* (Howard, 1981).

Potential proteins that need to be localised by mRNA transport in *U. maydis* include enzymes involved in cell wall synthesis, such as chitin synthases (Weber et al., 2003), components of the endocytosis machinery (Steinberg et al., 2001), regulatory proteins such as small G proteins (Mahlert et al., 2006), or cell-shape determinants such as septins (Boyce et al., 2005). The latter example is of particular interest, because septins were initially identified to function during septation in *S. cerevisiae* (Gladfelter, 2006) and localise at the hyphal tip as well as the distal septum in filaments of *Candida albicans* (Warenda and Konopka, 2002). The function of septins is consistent with our observation that *rrm4Δ* strains are impaired in septation and the predicted localisation pattern fits with our data that Rrm4-containing particles are moving to the apical as well as the distal pole of the hyphae.

The determination of polarity by shuttling of RNA-binding proteins along microtubules is a novel concept for fungal pathogens. It resembles RNA transport processes occurring during oogenesis, embryogenesis and neuronal processes in higher eukaryotes (Jansen and Kiebler, 2005; St Johnston, 2005). This suggests that the underlying fundamental principles of such microtubule-dependent long-distance transport are evolutionarily ancient.

Materials and Methods

Strains and growth conditions

E. coli K-12 derivatives DH5α (Bethesda Research Laboratories) and Top10 (Invitrogen) were used for cloning purposes. Growth conditions for *U. maydis* strains and source of antibiotics were described previously (Brachmann et al., 2004). *U. maydis* strains were constructed by transformation of progenitor strains with linearised plasmids (supplementary material Table S1). Homologous integration events at the *ip*, *kin1* or *rrm4* locus were verified by Southern blot analysis (Brachmann et al., 2004). For each experiment two independent transformants were analysed. Filamentous growth of AB33 derivatives was induced by shifting cells of an exponential growing culture (OD_{600}=0.4–0.5) from liquid complete medium to nitrate minimal medium (NM). Cells were incubated at 28°C shaking with 200 rpm. For filamentous growth on plates, cells were incubated at 20°C for 24 hours on NM medium, containing 10 g/l activated charcoal and 20 g/l Bacto™ agar.

Plasmids and plasmid constructions

Standard molecular techniques were followed. Plasmids pCR2.1-Topo (Invitrogen) and pBluescriptSKII (Stratagene) were used as cloning vehicles. Plasmid pRrm4Δ-HygR (pUMa495) was derived following published strategies to generate gene replacement mutants in *U. maydis* (Brachmann et al., 2004). 0.9 kb upstream and 1.9 kb downstream flanking sequences of the ORF region were amplified with primer combinations MF220/MF803 and MF804/MF805 (supplementary material Table S2), respectively. Genomic DNA of wild-type strain UM521 (*a1b1*) was used as template. Primers MF803 and MF804 introduced *Sfi*I(u) and *Sfi*I(d) recognition sites at the 3′ end of the upstream flanking region and the 5′ end of the downstream flanking region, respectively. PCR products were cleaved with *Sfi*I and ligated in the presence of a compatible 1.8 kb *Sfi*I(u)/*Sfi*I(d) fragment (pUMa194) containing the hygromycin-resistance cassette. The ligation product was cloned into pCR2.1-Topo. This plasmid was used to replace a 2376 bp region starting at nucleotide position –19 of the *rrm4* ORF (numbering relative to the translational start) by homologous integration of the hygromycin resistance cassette. Following the same strategy, plasmid pKin1Δ-HygR (pUMa542) was generated using *Sfi*I-cleaved PCR products that were amplified using primer combinations MF787/MF788 (1 kb upstream flanking region) and MF789/MF790 (1.5 kb downstream flanking region). MF788 and MF789 introduced *Sfi*I(u) and *Sfi*I(d) recognition sites at the 3′ end of the upstream flank and the 5′ end of the downstream flank, respectively. By homologous integration a 3036 bp region starting at nucleotide position 6 of the *kin1* ORF is replaced by the hygromycin resistance cassette.

For C-terminal fusion of Rrm4 with eGFP, we adapted the *Sfi*I-dependent gene replacement strategy (Brachmann et al., 2004) and constructed plasmid pRrm4G-NatR (pUMa496). This plasmid contains a 3.2 kb upstream flanking region including the 2.3 kb *rrm4* ORF as well as a 1.9 kb downstream flanking region. In addition it carried a 2.4 kb *Sfi*I(uC)/*Sfi*I(d) fragment derived from plasmid pMF5-1n (pUMa389) containing an *egfp* ORF in combination with a nourseothricin (Nat)-resistance cassette. Fusion was achieved by introducing a *Sfi*I(uC) recognition site at the C-terminus of Rrm4 performing a PCR with primers MF631 and MF220 as well as genomic DNA of wild-type strain UM521 (*a1b1*) as template. The *Sfi*I(uC) sequence GGCCAACGCGGCC encodes the amino acid sequence ANAA linking the ORFs of Rrm4 and eGFP.

Similarly, for C-terminal fusion of Rrm4 with mRFP, we constructed plasmid pRrm4R-NatR (pUMa520) containing a 3.2 kb upstream flanking region including the 2.3 kb *rrm4* ORF as well as a 1.9 kb downstream flanking region. In addition it carried a 2.4 kb *Sfi*I(uC)/*Sfi*I(d) fragment derived from plasmid pMF5-2n (pUMa738) containing the *mrfp* ORF in combination with a nourseothricin resistance cassette (Nat).

Plasmid pRrm4G$^{P\Delta}$-NatR (pUMa503) is comparable to plasmid pRrm4G-NatR (pUMa496). The only difference is a deletion in the *rrm4* ORF lacking 294 bp (from nucleotide position 2066 to 2359 relative to the ATG) encoding the PABC domain.

Plasmid pRrm4G^{mP}-NatR (pUMa607) is comparable to plasmid pRrm4G-NatR (pUMa496). It differs only in a mutated PABC domain (Fig. 4A). The mutations were introduced in pRrm4G-NatR (pUMa496) using primers MF737 and MF738.

Plasmids pRrm4G^{mR1}-NatR (pUMa634) and pRrm4G^{mR3}-NatR (pUMa637) are comparable to pRrm4G-NatR (pUMa496) but contain the *rrm4* ORF with mutations in the RNP1 regions of RRM1 and RRM3, respectively (Fig. 4A). Mutations mR1 and mR3 were introduced in pRrm4G-NatR (pUMa496) using primers MF750 and MF755, respectively.

For C-terminal fusion of eGFP and Tap tag we constructed plasmid pRrm4GT-NatR (pUMa603) containing a 3.2 kb upstream flanking region including the 2.3 kb *rrm4* ORF as well as a 1.9 kb downstream flanking region. In between these two regions a 3 kb *Sfi*I(uC)/*Sfi*I(d) fragment was inserted that was derived from plasmid pMF5-3n (pUMa737) containing the *egfp* ORF fused to a codon-optimised Tap tag (Rigaut et al., 1999) as well as a nourseothricin resistance cassette.

Plasmids pRrm4GT^{mP}-NatR (pUMa724), pRrm4GT^{mR1}-NatR (pUMa698) and pRrm4GT^{mR3}-NatR (pUMa700) were constructed by replacing the *Sfi*I(uC)/*Sfi*I(d) cassette derived from pMF5-1n with the corresponding one from pMF5-3n in plasmids pRrm4G^{mP}-NatR, pRrm4G^{mR1}-NatR, and pRrm4G^{mR3}-NatR, respectively.

All constructions were confirmed by sequencing and all plasmid sequences are available upon request.

Western blot analysis

Whole cell extracts for determination of Rrm4G derivatives in Western blot analysis were prepared from 10-20 ml of culture (OD_{600}=0.5). Cells were resuspended in 200 μl lysis buffer [100 mM sodium phosphate buffer, pH 8; 10 mM Tris-HCl, pH 8; 8 M urea; 1 mM PMSF; 0.5 mM benzamidine; 2× complete protease inhibitor cocktail (Roche)] and destroyed in the presence of glass beads in a pebble mill (Retsch, Germany) by shaking for 7.5 minutes at 30 times/second. After centrifugation (50,000 ***g*** for 5 minutes at RT) protein concentration of the supernatant was determined by Bradford assay (Bio-Rad) and 20 μg protein was resolved by SDS-PAGE and transferred to a PVDF membrane. Rrm4G derivatives were detected using anti-GFP antibody (Roche) (mixture of two mouse monoclonal antibodies directed against GFP) and anti-mouse IgG HRP conjugate (H+L; Promega) as primary and secondary antibodies, respectively. HRP activity was detected using the ECL plus western blotting detection system (Amersham Bioscience).

CLIP experiments

We used a modified CLIP procedure (Ule et al., 2003) replacing immunoprecipitation by tandem affinity purification (Rigaut et al., 1999). For each experiment 150 ml of cells were shifted in NM medium for 6 hours, harvested by centrifugation and resuspended in 5 ml UmTT buffer (100 mM sodium phosphate buffer, 0.1 % NP-40, 150 mM NaCl, 2 mM EDTA, 50 mM NaF, 0.1 mM Na_3VO_4, 10 mM DTT, 1 mM PMSF, 5 mM benzamidine, 2× complete protease inhibitor cocktail). Cells were irradiated in a 12-cm^2 Petri dish on ice with 4.8 J/cm^2 using a Stratalinker (Stratagene, wavelength 254 nm). 200 U RNasin (Promega) were added, cells were frozen in liquid nitrogen and treated for 15 minutes in a pebble

mill shaking 30 times/second. After centrifugation (20 minutes, 4°C, 50,000 ***g***), the supernatant was combined with 150 μl rabbit IgG agarose beads (Sigma) equilibrated with 500 μl UmTT buffer, and incubated for 60 minutes at 4°C on a turning wheel. Beads were washed three times with 1 ml IPP150 buffer (10 mM Tris-HCl, pH 8; 150 mM NaCl; 0.1% NP40; 50 mM DTT) and three times with TEV buffer (10 mM Tris-HCl, pH 8; 150 mM NaCl; 0.1% NP40; 0.5 mM EDTA; 1 mM DTT). Beads were resuspended in 150 μl TEV buffer, 50 U TEV protease (Invitrogen) and 40 U RNasin, and incubated for 90 minutes as above. After centrifugation, 300 μl supernatant (including a washing step with 150 μl TEV buffer) was combined with 900 μl CB buffer (10 mM Tris-HCl, pH 8; 150 mM NaCl; 0.1% NP40; 1 mM magnesium acetate; 1 mM imidazol; 2 mM $CaCl_2$; with 7.5 μl β-mercaptoethanol, 40 U RNasin and 1 μl 1 M $CaCl_2$ freshly added) and 50 μl calmodulin affinity resin (Stratagene) equilibrated with 500 μl CB buffer and incubated for 60 minutes as before. Beads were washed three times with 1 ml CB buffer and resuspended in 80 μl CB buffer. 40 U RNasin, 50 U RNase-free DNase (Roche) and 100 U (or 1 U) RNase T1 (Roche) were added before incubation for 10 minutes at 37°C with agitation for 30 seconds every 3 minutes. Beads were washed three times with 1 ml CB-PNK buffer (50 mM Tris-HCl, pH 8; 150 mM NaCl; 0.1% NP40; 10 mM magnesium acetate; 1 mM imidazol; 2 mM $CaCl_2$; 1 mM DTT) and resuspended in 80 μl CB-PNK buffer. 30 U calf intestinal alkaline phosphatase (New England Biolabs) and 40 U RNasin were added before incubating for 10 minutes at 37°C shaking for 30 seconds every 3 minutes at 1000 rpm. Beads were washed three times with 1 ml CB-PNK buffer and resuspended in 80 μl CB-PNK buffer. 40 U RNasin, 5 μl [γ-^{32}P]ATP (10 μCi/μl; Hartmann Analytics) and 50 U polynucleotide kinase (New England Biolabs) were added and incubated for 20 minutes at 37°C shaking as mentioned above. In the case of RNase A treatment, the concentration was adjusted to 2 mg/ml (RNase A, Qiagen) and beads were incubated for 10 minutes at 37°C. 10 μl ATP (10 mM) was added before incubating for 10 minutes at 37°C shaking as mentioned above. Beads were washed three times with 1 ml CB buffer and resuspended in 20 μl NuPAGE LDS sample buffer (Invitrogen) and incubated for 10 minutes at 70°C. Probes were analysed on 10% Bis-Tris gels (NuPAGE, Invitrogen) and transferred onto nitrocellulose membranes using protocols recommended by the manufacturer. Membranes were subjected to western analysis and phosphoimaging.

Inhibitor studies

1 ml cell suspension was incubated in the presence of either 100 μM CCCP, 50 μM latrunculin A or 20 μM benomyl (all from Sigma). Samples were incubated for 5-30 minutes at RT with agitation followed by microscopic analysis.

Microscopy, image processing and quantitative analysis

Cell suspensions were dropped onto glass slides covered with thin layer of agarose (1% w/v) and analysed using a Zeiss Axioplan II microscope. Epifluorescence was observed using FITC (BP500/20, FT515, BP535/30), RFP (HQ565/30, Q585, HQ620/60) or DAPI (BP365/12, FT395, LP397) filter sets. Filters were obtained from Carl Zeiss AG or AF Analysetechnik. Frames were taken with a cooled CCD-camera (CoolSNAP HQ, Roper Scientific) controlled by MetaMorph (Universal Imaging). For co-localisation studies in vivo eGFP and mRFP frames were taken with switching intervals of 430 mseconds using a filter wheel (Visitron Systems) equipped with excitation filters for GFP (BP480/25), RFP (BP 565/25) and a dual-band mirror (GFP: FT 480, BP503-545; RFP: FT565, BP591-647). Measurements and image processing, including adjustment of brightness, contrast and gamma values were performed with MetaMorph and Photoshop 6.0 (Adobe). The number of particles and their velocity were measured 6 hours after shifting cells into NM medium. Particle density in filaments was determined in a 20-μm region at a distance of 10 μm from the growing tip. Relative intensity of particle fluorescence was determined by measuring pixels using a mask of 0.28 μm^2. To determine the maximal length of tip cells, the distance between tip and distal end was measured 6 hours after induction of filament formation. Since cells were not synchronised, filament initiation was not uniform, resulting in a high bandwidth of filament length. To filter those cells that reacted late we only evaluated those cells whose length exceeded the median.

We acknowledge C. Julius, K. Zarnack, A. Brachmann, R. Kahmann as well as lab members for valuable discussion and critical reading of the manuscript. We thank G. Steinberg and R. Fischer for helpful discussions on cell biological aspects, J. Ule for advice on CLIP, as well as J. Hohenner for excellent technical assistance. We are grateful to M. Treutlein and J. Kämper for the codon-optimised Tap tag. Grants from Bayer CropScience and the Deutsche Forschungsgemeinschaft to M.F. (FE 448/3) supported this work.

References

Abe, R., Sakashita, E., Yamamoto, K. and Sakamoto, H. (1996). Two different RNA binding activities for the AU-rich element and the poly(A) sequence of the mouse neuronal protein mHuC. *Nucleic Acids Res.* **24**, 4895-4901.

Albrecht, M. and Lengauer, T. (2004). Survey on the PABC recognition motif PAM2. *Biochem. Biophys. Res. Commun.* **316**, 129-138.

Anderson, P. and Kedersha, N. (2006). RNA granules. *J. Cell Biol.* **172**, 803-808.

Banerjee, H., Rahn, A., Gawande, B., Guth, S., Valcarcel, J. and Singh, R. (2004). The conserved RNA recognition motif 3 of U2 snRNA auxiliary factor (U2AF 65) is essential *in vivo* but dispensable for activity *in vitro*. *RNA* **10**, 240-253.

Becht, P., Vollmeister, E. and Feldbrügge, M. (2005). A role for RNA-binding proteins implicated in pathogenic development of *Ustilago maydis*. *Eukaryotic Cell* **4**, 121-133.

Boyce, K. J., Chang, H., D'Souza, C. A. and Kronstad, J. W. (2005). An *Ustilago maydis* septin is required for filamentous growth in culture and for full symptom development on maize. *Eukaryotic Cell* **4**, 2044-2056.

Brachmann, A., Weinzierl, G., Kämper, J. and Kahmann, R. (2001). Identification of genes in the bW/bE regulatory cascade in *Ustilago maydis*. *Mol. Microbiol.* **42**, 1047-1063.

Brachmann, A., König, J., Julius, C. and Feldbrügge, M. (2004). Reverse genetic approach for generating gene replacement mutants in *Ustilago maydis*. *Mol. Genet. Genomics* **272**, 216-226.

Campbell, R. E., Tour, O., Palmer, A. E., Steinbach, P. A., Baird, G. S., Zacharias, D. A. and Tsien, R. Y. (2002). A monomeric red fluorescent protein. *Proc. Natl. Acad. Sci. USA* **99**, 7877-7882.

Carris, L. M., Castlebury, L. A. and Goates, B. J. (2006). Nonsystemic Bunt Fungi-*Tilletia indica* and *T. horrida*: a review of history, systematics, and biology. *Annu. Rev. Phytopathol.* **44**, 113-133.

Deardorff, J. A. and Sachs, A. B. (1997). Differential effects of aromatic and charged residue substitutions in the RNA binding domains of the yeast poly(A)-binding protein. *J. Mol. Biol.* **269**, 67-81.

Deo, R. C., Bonanno, J. B., Sonenberg, N. and Burley, S. K. (1999). Recognition of polyadenylate RNA by the poly(A)-binding protein. *Cell* **98**, 835-845.

Dreyfuss, G., Kim, V. N. and Kataoka, N. (2002). Messenger-RNA-binding proteins and the messages they carry. *Nat. Rev. Mol. Cell Biol.* **3**, 195-205.

Feldbrügge, M., Kämper, J., Steinberg, G. and Kahmann, R. (2004). Regulation of mating and pathogenic development in *Ustilago maydis*. *Curr. Opin. Microbiol.* **7**, 666-672.

Fuchs, U., Manns, I. and Steinberg, G. (2005). Microtubules are dispensable for the initial pathogenic development but required for long-distance hyphal growth in the corn smut fungus *Ustilago maydis*. *Mol. Biol. Cell* **16**, 2746-2758.

Gladfelter, A. S. (2006). Control of filamentous fungal cell shape by septins and formins. *Nat. Rev. Microbiol.* **4**, 223-229.

Handa, N., Nureki, O., Kurimoto, K., Kim, I., Sakamoto, H., Shimura, Y., Muto, Y. and Yokoyama, S. (1999). Structural basis for recognition of the tra mRNA precursor by the Sex-lethal protein. *Nature* **398**, 579-585.

Harris, S. D., Read, N. D., Roberson, R. W., Shaw, B., Seiler, S., Plamann, M. and Momany, M. (2005). Polarisome meets spitzenkörper: microscopy, genetics, and genomics converge. *Eukaryotic Cell* **4**, 225-229.

Howard, R. J. (1981). Ultrastructural analysis of hyphal tip cell growth in fungi: spitzenkorper, cytoskeleton and endomembranes after freeze-substitution. *J. Cell Sci.* **48**, 89-103.

Hull, C. M. and Heitman, J. (2002). Genetics of *Cryptococcus neoformans*. *Annu. Rev. Genet.* **36**, 557-615.

Jansen, R. P. and Kiebler, M. (2005). Intracellular RNA sorting, transport and localization. *Nat. Struct. Mol. Biol.* **12**, 826-829.

Kämper, J., Reichmann, M., Romeis, T., Bölker, M. and Kahmann, R. (1995). Multiallelic recognition: nonself-dependent dimerization of the bE and bW homeodomain proteins in *Ustilago maydis*. *Cell* **81**, 73-83.

Kozlov, G., Trempe, J. F., Khaleghpour, K., Kahvejian, A., Ekiel, I. and Gehring, K. (2001). Structure and function of the C-terminal PABC domain of human poly(A)-binding protein. *Proc. Natl. Acad. Sci. USA* **98**, 4409-4413.

Kozlov, G., De Crescenzo, G., Lim, N. S., Siddiqui, N., Fantus, D., Kahvejian, A., Trempe, J. F., Elias, D., Ekiel, I., Sonenberg, N. et al. (2004). Structural basis of ligand recognition by PABC, a highly specific peptide-binding domain found in poly(A)-binding protein and a HECT ubiquitin ligase. *EMBO J.* **23**, 272-281.

Lehmler, C., Steinberg, G., Snetselaar, K. M., Schliwa, M., Kahmann, R. and Bölker, M. (1997). Identification of a motor protein required for filamentous growth in *Ustilago maydis*. *EMBO J.* **16**, 3464-3473.

Lenz, J. H., Schuchardt, I., Straube, A. and Steinberg, G. (2006). A dynein loading zone for retrograde endosome motility at microtubule plus-ends. *EMBO J.* **25**, 2275-2286.

Ma, W. J., Chung, S. and Furneaux, H. (1997). The Elav-like proteins bind to AU-rich elements and to the poly(A) tail of mRNA. *Nucleic Acids Res.* **25**, 3564-3569.

Mahlert, M., Leveleki, L., Hlubek, A., Sandrock, B. and Bolker, M. (2006). Rac1 and Cdc42 regulate hyphal growth and cytokinesis in the dimorphic fungus *Ustilago maydis*. *Mol. Microbiol.* **59**, 567-578.

Maris, C., Dominguez, C. and Allain, F. H. (2005). The RNA recognition motif, a plastic RNA-binding platform to regulate post-transcriptional gene expression. *FEBS J.* **272**, 2118-2131.

Moore, M. J. (2005). From birth to death: the complex lives of eukaryotic mRNAs. *Science* **309**, 1514-1518.

Ralser, M., Albrecht, M., Nonhoff, U., Lengauer, T., Lehrach, H. and Krobitsch, S. (2005). An integrative approach to gain insights into the cellular function of human ataxin-2. *J. Mol. Biol.* **346**, 203-214.

Rigaut, G., Shevchenko, A., Rutz, B., Wilm, M., Mann, M. and Seraphin, B. (1999).

A generic protein purification method for protein complex characterization and proteome exploration. *Nat. Biotechnol.* **17**, 1030-1032.

Schuchardt, I., Assmann, D., Thines, E., Schuberth, C. and Steinberg, G. (2005). Myosin-V, Kinesin-1, and Kinesin-3 cooperate in long-distance transport in hyphal growth of the fungus *Ustilago maydis*. *Mol. Biol. Cell* **16**, 5191-5201.

St Johnston, D. (2005). Moving messages: the intracellular localization of mRNAs. *Nat. Rev. Mol. Cell Biol.* **6**, 363-375.

Steinberg, G. and Fuchs, U. (2004). The role of microtubules in cellular organization and endocytosis in the plant pathogen *Ustilago maydis*. *J. Microsc.* **214**, 114-123.

Steinberg, G., Schliwa, M., Lehmler, C., Bolker, M., Kahmann, R. and McIntosh, J. R. (1998). Kinesin from the plant pathogenic fungus *Ustilago maydis* is involved in vacuole formation and cytoplasmic migration. *J. Cell. Sci.* **111**, 2235-2246.

Steinberg, G., Wedlich-Söldner, R., Brill, M. and Schulz, I. (2001). Microtubules in the fungal pathogen *Ustilago maydis* are highly dynamic and determine cell polarity. *J. Cell. Sci.* **114**, 609-622.

Ule, J., Jensen, K. B., Ruggiu, M., Mele, A., Ule, A. and Darnell, R. B. (2003). CLIP identifies Nova-regulated RNA networks in the brain. *Science* **302**, 1212-1215.

Ule, J., Jensen, K., Mele, A. and Darnell, R. B. (2005). CLIP: a method for identifying protein-RNA interaction sites in living cells. *Methods* **37**, 376-386.

Wang, X. and Tanaka Hall, T. M. (2001). Structural basis for recognition of AU-rich element RNA by the HuD protein. *Nat. Struct. Biol.* **8**, 141-145.

Warenda, A. J. and Konopka, J. B. (2002). Septin function in *Candida albicans* morphogenesis. *Mol. Biol. Cell* **13**, 2732-2746.

Weber, I., Gruber, C. and Steinberg, G. (2003). A class-V myosin required for mating, hyphal growth, and pathogenicity in the dimorphic plant pathogen *Ustilago maydis*. *Plant Cell* **15**, 2826-2842.

Wedlich-Söldner, R., Bölker, M., Kahmann, R. and Steinberg, G. (2000). A putative endosomal t-SNARE links exo- and endocytosis in the phytopathogenic fungus *Ustilago maydis*. *EMBO J.* **19**, 1974-1986.